

Mechanism and Elimination of Scan Blindness in a T-Printed Dipole Array

Hanni Koo¹ and Sangwook Nam¹, *Senior Member, IEEE*

Abstract—In this article, the scan blindness in a T-printed dipole is analyzed, and an elimination strategy is proposed. First, the main cause of scan blindness is analyzed. The scan characteristics are obtained using an active element pattern (AEP) with an infinite rectangular lattice arrangement. Based on the propagation of a guided wave along the antenna row and the electric-field (E -field) distribution observed during simulations, an equivalent circuit model for a unit cell of the T-printed dipole is obtained. A quasi-transverse electromagnetic (TEM) guided wave is predicted using the dispersion relation curve obtained from the equivalent circuit, and it is proven that the calculated curve is in good agreement with the eigen mode simulations and measured trajectory of the scan blind angle, for different frequencies. Next, slits and stubs are introduced as parasitic structures to eliminate the scan blindness and improve the antenna scan range. To confirm the effects of these parasitic elements, a linear array simulation is performed, which confirms the suppression of a quasi-TEM guided wave. Analysis of the active reflection coefficient and dispersion diagram indicates that the scan characteristics have been improved by the addition of parasitics. Four types of array prototypes are fabricated and their measurements validate the scan blindness prediction and confirm the proposed mechanism of scan blindness and its improvements.

Index Terms—Phased array, quasi-transverse electromagnetic (TEM) guided wave, scan blindness, T-printed dipole.

I. INTRODUCTION

SCAN blindness is a critical issue in phased array antennas. If an infinite phased array structure is capable of supporting a guided wave, then under certain Floquet excitations, the amplitude of the guided mode field infinitely increases, resulting in infinitely large input impedance. Thus, the array ceases to radiate. This phenomenon is known as scan blindness and the corresponding angle at which this occurs is called the blind angle [1]. Comprehensive studies have been conducted on the scan blindness in planar printed antennas such as dipoles or rectangular microstrip patches, based on the coupling from Floquet modes to surface-wave modes [2]–[5]. However, scan blindness is caused by not only surface waves but also various other factors. In 1991, infinite arrays of printed dipoles on finite-height dielectric sheet were

analyzed using Green's function moment method approach and mode matching and its scan blindnesses were observed in the E -plane [6]. In 1994, the E -plane scan results were presented for infinite arrays of microstrip-fed dipoles printed on protruding dielectric substrates [7]. In 1996, a model of parallel-plate modes was proposed to predict the existence and location of the E -plane scan blindness in a tapered-slot single-polarized array, which is associated with a guided wave on a corrugated surface [8]. In 2008, the scan blindness in single polarized tapered-slot elements in triangular grids was explained to have occurred because of the presence of leaky waves in the structure [9].

Various methods have been proposed to reduce the scan blindness in phased arrays, depending on the antenna element geometry [10]–[16]. The electromagnetic bandgap (EBG) structure is an effective method to eliminate scan blindness by suppressing the surface waves generated in printed phased arrays, and many related methods have been proposed [10]–[14]. Studies have been conducted to eliminate the scan blindness in Vivaldi arrays [15], [16]. In 2014, triangular parasitic notches were proposed to reduce the magnitude of leaky modes for E -plane scanning and shift the cavity resonances of stripline-fed tapered-slot antennas to higher frequencies [15]. In 2018, a sliced notch antenna (SNA) array was proposed, which offered better suppression of the classical Vivaldi E -plane scan blindness [16].

In this article, the mechanism of scan blindness in a T-printed dipole array is described, and an effective scan blindness elimination strategy is proposed. A T-printed dipole with integrated balun has been proposed for wireless communication at microwave frequencies [17]–[24], because it has many advantages such as lightweight, low cost, ease of fabrication, and suitability for integration with microwave integrated circuit modules. The T-printed dipole structure can support a wave that propagates along the E -plane, which resembles the quasi-transverse electromagnetic (TEM) mode of a rectangular mushroom structure proposed in [25]. Furthermore, this quasi-TEM analysis has been used to quickly and accurately calculate the dispersion curves [26].

Scan blindness is observed using an active element pattern (AEP) and active reflection coefficient [1], [27]. From the electric field (E -field) distribution at the scan blind angle in the E -plane, an equivalent circuit model for a unit cell is proposed and the equation for the dispersion relations is derived using the transmission line (TL) theory [26], [28], which has been successfully used to calculate the dispersion relations for 2-D periodic structures [29], [30]. The dispersion diagram is also

Manuscript received March 17, 2019; revised July 22, 2019; accepted July 28, 2019. Date of publication August 19, 2019; date of current version January 3, 2020. This work was supported in part by the National Research Foundation of Korea through the Korea Government [Ministry of Science, ICT and Future Planning (MSIP)] under Grant 2016R1E1A1A01943375 and in part by Hanwha System. (Corresponding author: Sangwook Nam.)

The authors are with the School of Electrical and Computer Engineering, Institute of New Media Communication, Seoul National University, Seoul 152-742, South Korea (e-mail: hnkoo@ael.snu.ac.kr; snam@snu.ac.kr).

Color versions of one or more of the figures in this article are available online at <http://ieeexplore.ieee.org>.

Digital Object Identifier 10.1109/TAP.2019.2935132

0018-926X © 2019 IEEE. Personal use is permitted, but republication/redistribution requires IEEE permission. See http://www.ieee.org/publications_standards/publications/rights/index.html for more information.

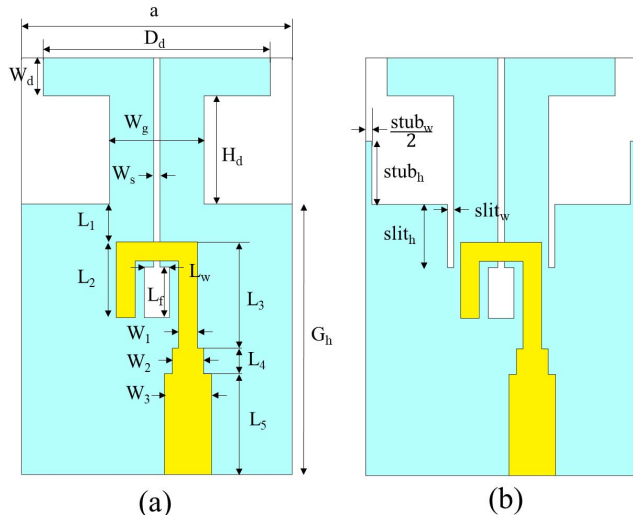


Fig. 1. Geometry of an element. (a) Basic T-printed dipole. (b) T-printed dipole with slits and stubs.

used to verify the existence of the guided mode in the T-printed dipole, which is a proper method to find resonant frequencies in periodic structures.

We propose the T-printed dipole model to eliminate the guided wave effect and compare it to the conventional model. In 2015, a radio frequency choke (RFC) using modified stubs was developed to improve the isolation characteristics of multiple input multiple output (MIMO) antennas [31]. In 2017, Ta *et al.* [23] and Ta and Park [24] proposed inserting a microstrip stub between two printed angled-dipole antennas to improve the scanning angle range, bandwidth, radiation efficiency, and mutual coupling. However, the specific mechanism by which the stub could reduce the mutual coupling and widen the scan range is not explained. In this article, the role of slits and stubs is discussed in terms of the scan blindness and suppression of the guided wave. These parasitic elements are applied to the T-printed dipole to effectively eliminate scan blindness.

The remainder of this article is organized as follows. In Section II, the T-printed dipole element structure and requirements are introduced. Section III presents an analysis of the scan blindness effect in an infinite array. Based on this analysis, an equivalent circuit model is explained. Section IV shows that the proposed model supports guided-wave suppression along the printed dipole array in the E-plane. The dispersion diagram is used to validate the proposed idea. Section V presents the simulation model and the fabrications of four types of T-printed dipole antennas, with their measurement results. The conclusions are presented in Section VI.

II. SINGLE-ELEMENT DESIGN

A T-printed dipole element has low profile, lightweight, low cost, and compact size and is widely used for building phased arrays [21], [22]. Fig. 1 shows the configurations of a basic T-printed dipole element and the proposed one. These models are modified from the original model proposed in [23]. The substrate used in the proposed design is RT/Duroid Rogers

TABLE I
DESIGN PARAMETERS OF T-PRINTED DIPOLE ELEMENT

D_a	W_d	W_g	W_s	W_{h1}	W_{h2}	W_{h3}
3.6	0.6	1.5	0.01	1.29	0.4	1.6
W_1	W_2	W_3	L_f	L_w	L_1	L_1
0.3	0.5	0.74	0.8	0.4	0.6	1.2
G_h	$stub_h$	$stub_w$	$slits_h$	$slit_w$	G_h	a
4.285	1	0.1	1	0.1	4.285	4.285

(Unit: mm)

5880 with a relative permittivity of 2.2 and dielectric loss tangent of 0.009. The thickness of the dielectric and copper are 0.254 and 0.017 mm, respectively. The feedline consists of a microstrip and the balun, which are printed on the front of the substrate. The dipole and the ground are at the back of the substrate. Impedance matching is achieved by adjusting the folded line and the gap of the slot (W_s). The design values for the geometric parameters of the structure are described in Table I. In order to improve the E-plane scanning characteristics of the printed dipole array, stubs and slits are added between the two printed dipole antennas in the proposed design, as illustrated in Fig. 1(b). The length of the stub is determined in accordance with Alhalabi and Rebeiz [22]. Slits are added at both sides of the feedline to the T-printed dipole element to complement the stubs. The role of the parasitic elements is described in detail in Section IV.

III. SCAN BLINDNESS ANALYSIS

A. Active Element Pattern in Infinite Array

The AEP is a good indicator for predicting the scan blindness of a phased array [1], [27]. The patterns used in our work are obtained using an electromagnetic simulator, CST Microwave Studio. A rectangular lattice is selected, with an element spacing “ a ” of $0.5\lambda_0$ (where λ_0 is the free space wavelength) in the E-plane and H-plane, to avoid a grating lobe. The AEP in an infinite array for a basic T-printed dipole is obtained in the E-plane and H-plane as shown in Fig. 2(a). The pattern in the E-plane shows scan blindness at $\pm 36^\circ$ and sharply decays near the blind angle, which is quite different from the behavior of the H-plane pattern. Fig. 2(b) illustrates the AEP in an infinite array with slits and stubs. The scan blindness in the E-plane is eliminated, and the pattern in the H-plane shows little change when compared to Fig. 2(a).

B. E-Field Distribution in Infinite Array

The E-field distribution in the infinite array is obtained by Floquet excitation. Fig. 3(a) shows the E-field distribution in the infinite array when Floquet excitation is performed such that the incident angle is the blind angle. Fig. 3(b) illustrates the E-field distribution when the elements are excited with uniform amplitudes without phase progression to steer the bore sight angle. The amplitude of the E-field in Fig. 3(a) is considerably higher than that in Fig. 3(b). The E-field in Fig. 3(a) is strongly coupled between two dipole arms and it is different from the fields at the other angles. When scan

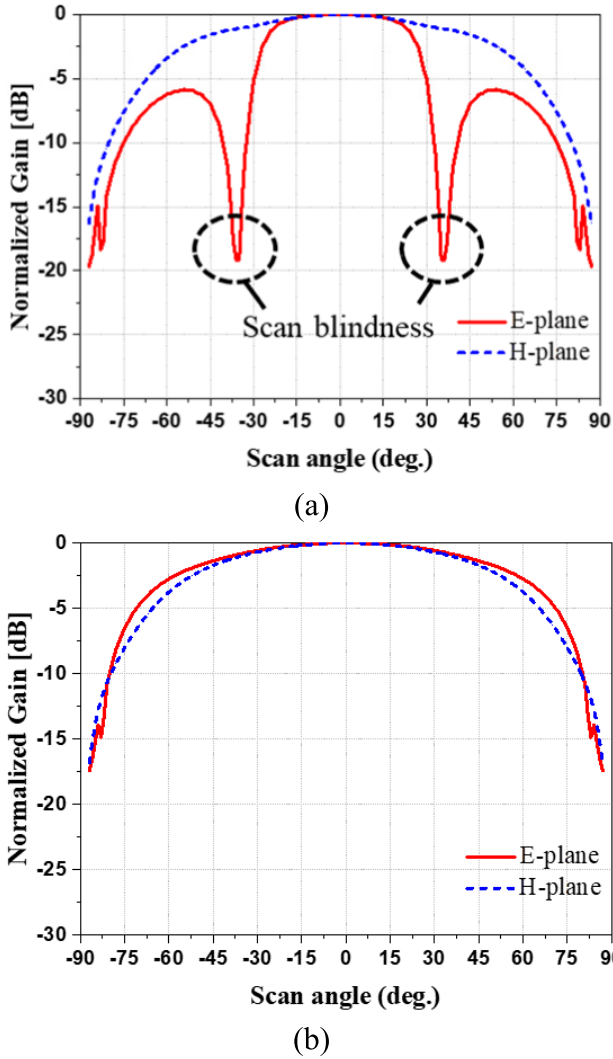


Fig. 2. AEP in an infinite array (comparison of the E-plane and H-plane). (a) Basic T-printed dipole. (b) T-printed dipole with slits and stubs.

blindness occurs, only the z -direction component of the E -field is present, and the wave propagates in the x -direction. Thus, the dipole arms and ground plane operate as a TL. These guiding fields are described as the quasi-TEM mode.

C. Dispersion Diagram

To understand the relationship between the scan blindness and the dispersion properties of a unit cell of the basic T-printed dipole element, two types of simulations were carried out. The first simulated a trajectory of the scan blindness for an AEP in an infinite array, according to the frequency change. The AEP is expressed in terms of the active reflection coefficient, also known as the Floquet reflection coefficient (Γ^{FL}) if no grating lobe exists for the infinite array under Floquet excitation [29]. Thus, the active element gain G_{AEP} could be expressed as

$$G_{AEP} = \frac{4\pi A_{unitcell}}{\lambda_0^2} \cos\theta \times [1 - |\Gamma^{FL}|] \quad (1)$$

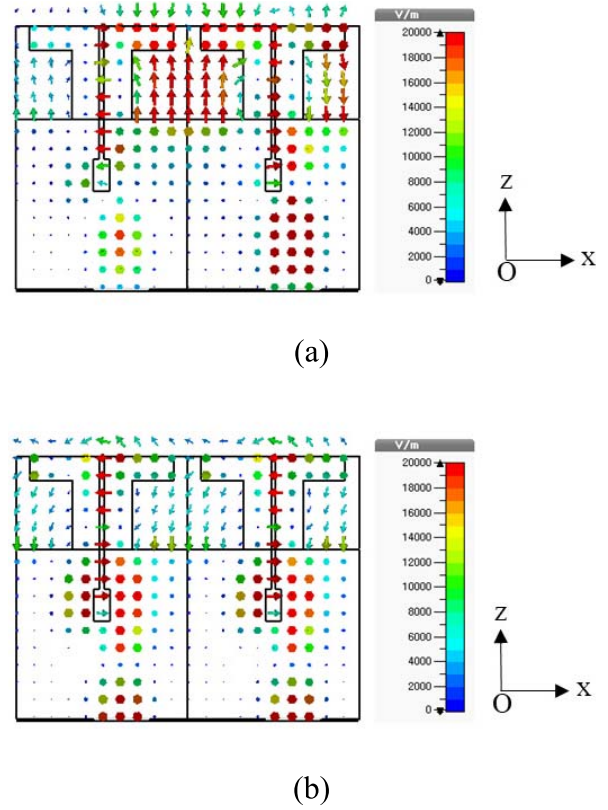


Fig. 3. E -field distribution between two dipoles in infinite array when Floquet excitation is performed so that the incident angle is (a) blind angle (36°) and (b) boresight angle (0°).

where $A_{unitcell}$ is a unit cell area. The scan blind angle can be verified from the singularity point traces of the active reflection coefficient in the infinite array, by sweeping the frequencies. Under such a condition, the amplitude of the guided wave increases, resulting in a very large input impedance and very poor matching. Thus, the active reflection coefficient converges to one, causing scan blindness [1]. The second is an eigen mode simulation to determine the resonances and dispersion properties of the unit cell. For the eigen mode analysis, the periodic boundary conditions (PBCs) are applied in both the x - and y -directions with a unit cell size “ a ” (4.285 mm). Only the phase shift along the x -direction is considered because of the E-plane scanning. The trajectories of the scan blindness and dispersion properties are in good agreement, as shown in Fig. 4. The relationship between a propagation constant of the unit cell (β_{unit}) and a scan angle (θ_{scan}) can be expressed as

$$\beta_{unit} = k_0 \sin\theta_{scan}. \quad (2)$$

In the dispersion diagram obtained from the eigen mode simulation, when the scan angle is 36° , the resonant frequency is 35 GHz, which corresponded to the scan blindness shown in Fig. 2. These results support the hypothesis that the propagation constant of a TEM guided mode coincides with that of a radiation mode, then two modes lead to a resonance and subsequent scan blindness.

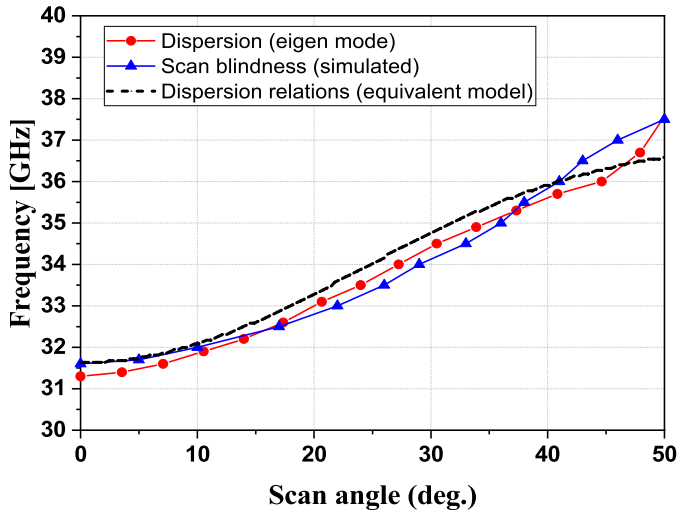


Fig. 4. Simulated dispersion diagrams of eigen mode, trajectory of scan blindness, and calculated dispersion relations obtained from (12).

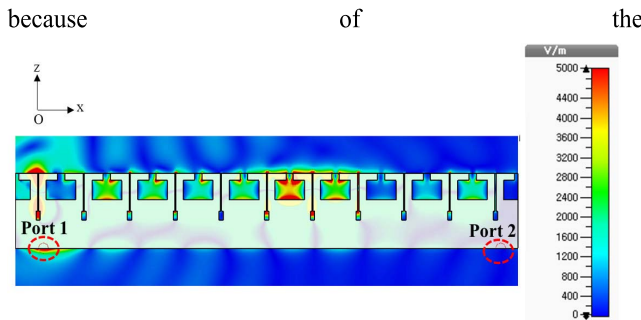


Fig. 5. E -field distribution of coupling between linear infinite dipole arrays placed 10 unit cells apart at 35 GHz for basic T-printed dipole array.

D. Guided Quasi-TEM mode

To support the guiding of the quasi-TEM mode, Fig. 5 shows the E -field simulation of the coupling between linear infinite dipole arrays placed 10 unit cells apart, describing the E -field magnitude of a T-printed dipole array in the E -plane. The PMC boundary to the y -direction is applied using the CST simulator to implement an infinite array. Ports are set on both sides of the 11-element array in the x -direction. Port 1 is excited to examine the E -field distribution guided along the antenna. It is observed that the guided wave is traveling in the direction of the antenna row when the antenna elements are coupled to each other. This simulation shows that the row of T-printed dipoles operates as a TL supporting the quasi-TEM mode.

E. Equivalent Circuit

Based on the observation of the dispersion properties in Fig. 4 and the quasi-TEM wave propagation to the x -direction in Fig. 5, the basic topology of the unit cell could be expressed as shown in Fig. 6(a). For simplicity, only a 1-D equivalent circuit is considered, as the propagation constant $\beta_y = 0$ in the E -plane direction [26]. This topology is composed of a series capacitance, TL, and transformer. Its

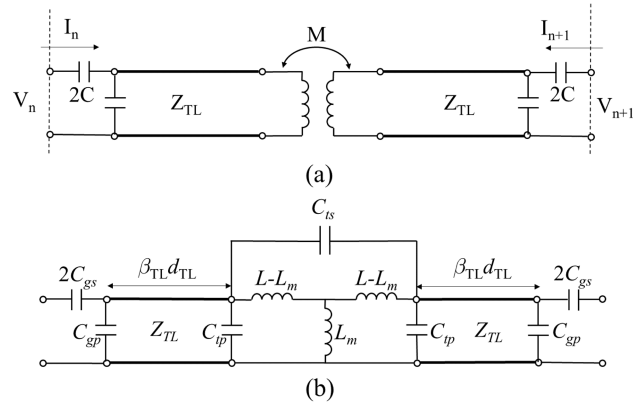


Fig. 6. (a) Equivalent topology of a T-printed dipole unit cell. (b) Transformed equivalent circuit.

equivalent circuit is depicted in Fig. 6(b). A gap capacitance for series (C_{gs}) is characterized between two adjacent printed dipole arms and a gap capacitance for parallel (C_{gp}) occurs due to discontinuity from the edge. The printed dipole arms are considered to be similar to a TL along the x -direction, forming a quasi-TEM mode, which is described by the characteristic impedance Z_{TL} and propagation constant β_{TL} of the TL. The E -field is coupled to the adjacent dipole through the feeding line and the energy is guided along the row of antenna elements, as shown in Fig. 5. Hence, the antenna feeding network operates as a transformer. A mutual inductance (L_m) and self-inductance (L) are used to represent the transformer. C_{tp} is a parasitic shunt capacitance arising from the discontinuity between the TL and transformer. C_{ts} is a parasitic series capacitance that occurs because of the antenna feeding line. Using the equivalent circuit proposed in Fig. 6(b), the equation for the dispersion relation is derived based on the TL theory [26]. β_{unit} is determined using the 1-D periodic circuit network according to [26] and [28]. The components in the unit cell are extracted from the ABCD matrix using the simulator and de-embedding methods [28]. Using the values of the elements obtained in Appendix, the dispersion relation curve is obtained as the dashed line in Fig. 4, which is compared with the trajectory of the scan blindness (blue line) and the eigen mode curve (red line). As the scan angle increases, the theoretically calculated results differ from the simulated or measured results. This could be because the quasi-TEM mode and the higher order mode are considered for the eigen mode simulated results, whereas the theoretical curves support only the quasi-TEM assumption. Within 45° , the calculation results fit well with those of the measurement and simulation.

IV. PARASITIC SLITS AND STUBS FOR ELIMINATING SCAN BLINDNESS

To improve the scan performance of the printed dipole array, in the E -plane direction, a slit and stub structure are proposed, as shown in Fig. 1(b). The effect of the parasitic elements is confirmed by the active reflection coefficient and E -field distribution of the quasi-TEM guided wave. The resonance

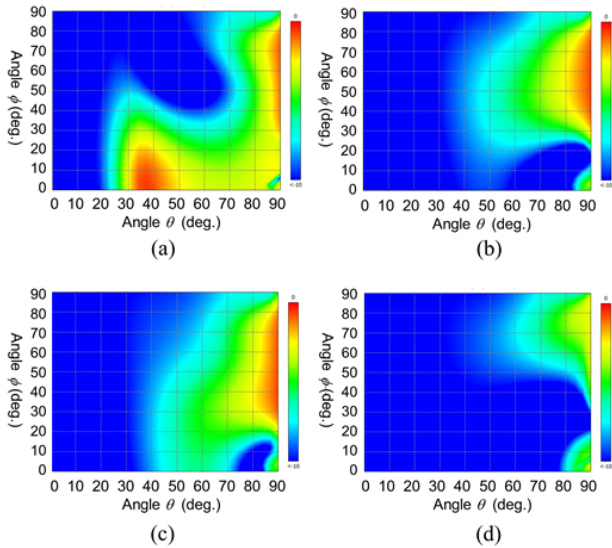


Fig. 7. Comparison of four types of 2-D active reflection coefficients. (a) Basic T-printed dipole. (b) With stubs. (c) With slits. (d) With slits and stubs.

frequencies of the guiding mode, with and without the parasitic structures, are verified using the dispersion diagram.

A. Comparison of Active Reflection Coefficients

The simulated active reflection coefficients for four cases in the 2-D infinite array are shown in Fig. 7. The blue part indicates that the active reflection coefficient is less than -10 dB. Fig. 7(a) indicates that reflection occurs around $\phi = 0^\circ$ and $\theta = \pm 36^\circ$ for a basic T-printed dipole, which is the scan blindness in the E-plane. To eliminate the scan blindness effect, three configurations of parasitics are considered. The first case is an element with stub, as depicted in Fig. 7(b). The second case is an element with slit, as depicted in Fig. 7(c). The third case is the elements with slits and stubs, shown in Fig. 7(d). The graph shows that the reflection coefficient is less than -10 dB for all Φ directions and θ within $\pm 45^\circ$, which is the best case among the four types in Fig. 7.

B. Guiding Wave Suppression

The presence of a guided wave is discussed in Section III. To observe the changes to the guided wave, caused by the parasitic structures, slits and stubs are added to the original array model depicted in Fig. 5. When port 1 is excited, the amplitude of the E -field in the proposed array is suppressed, as shown in Fig. 8. This indicates that the stubs and slits play a significant role in impeding the quasi-TEM guided wave along the printed dipole array in the E-plane. An S-parameter graph is depicted in Fig. 9. Fig. 9(a) describes the S-parameter characteristics for Fig. 5. The transmission coefficient is improved from -25 to -35 dB at 35 GHz, as shown in Fig. 9(b). Decreasing the amplitude of the guided wave, using parasitic structures, reduced the mutual coupling and improved the return loss.

C. Comparison of Dispersion Relations

To understand the propagation and suppression characteristics of the guided wave along the printed dipole, a dispersion

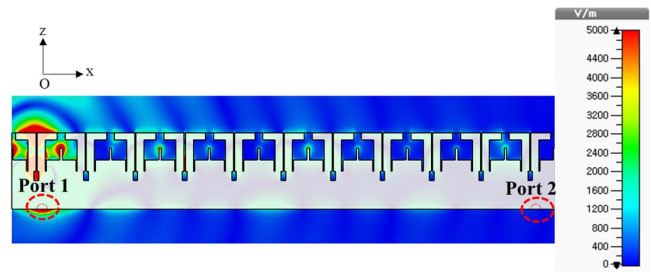


Fig. 8. E-field distribution of coupling between linear infinite dipole arrays placed 10 unit cells apart at 35 GHz for T-printed dipole with slits and stubs.

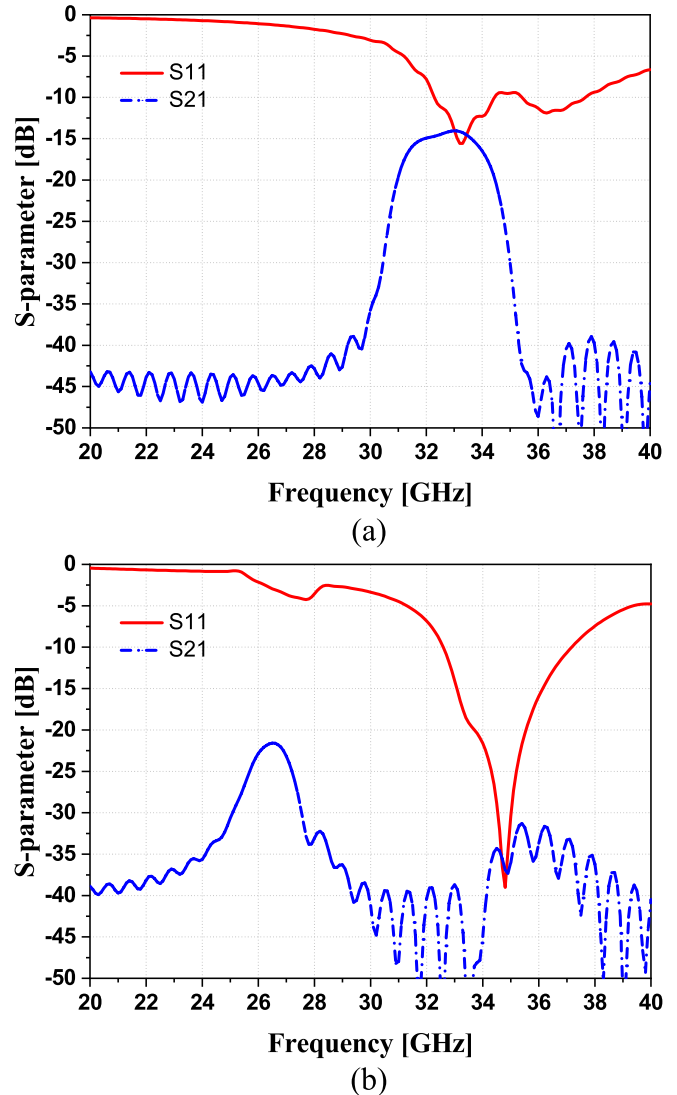


Fig. 9. S-parameter comparison of (a) basic T-dipole array, from Fig. 5, and (b) T-dipole with slits and stubs as parasitic structures, from Fig. 8.

diagram is used, as described in Section IV. The dispersion diagram shown in Fig. 10 is the result of parametric studies on the length of slits and stubs. The idea of inserting stub structures between printed dipoles is proposed in [23]; these can be equalized with an LC resonator to suppress leakage current [31]. The stubs and slits are characterized by a shunt

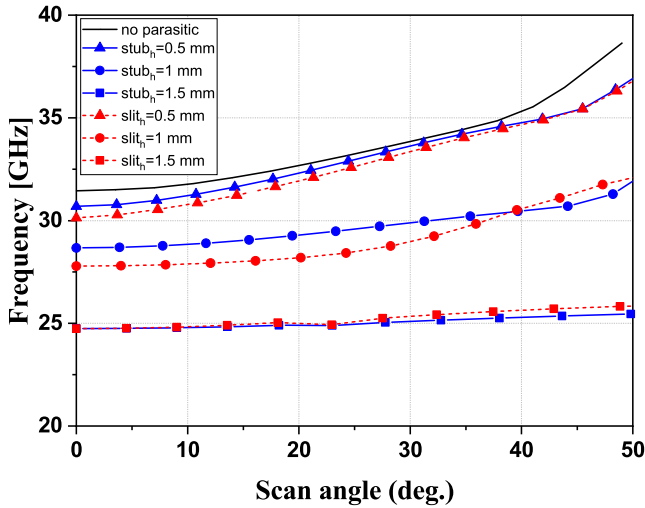


Fig. 10. Simulated dispersion diagram of eigen mode for different length of the slit ($slit_h$) and stub ($stub_h$).

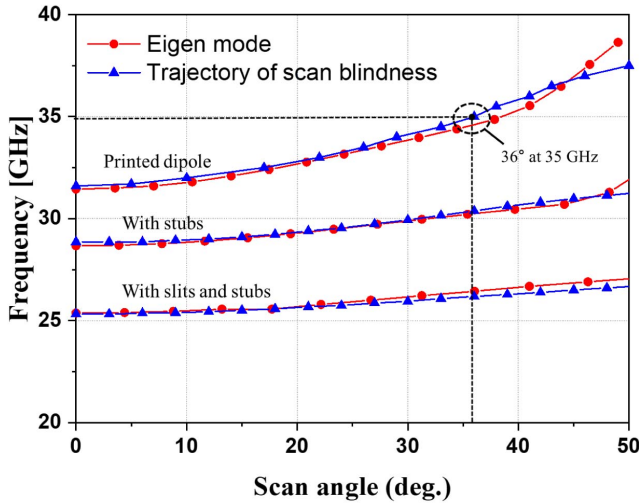


Fig. 11. Simulated dispersion diagram of eigen mode and trajectory of scan blindness. Three cases are compared: printed dipole versus printed dipole with stub versus printed dipole with slits and stubs.

capacitance (C_{shunt}) and series inductance (L_{series}), respectively. As L_{series} and C_{shunt} are added, β_{unit} is increased, which has the effect of lowering the resonance frequency of the quasi-TEM mode. Consequently, as the length of the stub or slit becomes longer in Fig. 10, C_{shunt} or L_{series} increases, such that the dispersion curve moves toward lower frequencies. At this time, if the length of the slit or stub exceeds 1 mm, the parasitic structure acts as a resonator, which affects the radiation pattern. Thus, the length of the parasitic element is determined to be 1 mm in order to avoid the resonance of the quasi-TEM mode at a given design frequency. Fig. 11 shows the results of the trajectory of scan blindness in an infinite array and the simulated dispersion diagram of eigen modes for the three structures. The first structure is a basic printed dipole element. The second is a unit cell with stubs. The third structure is one wherein the stubs and slits are inserted in a unit cell, supplementing the stub structures. The third case shows

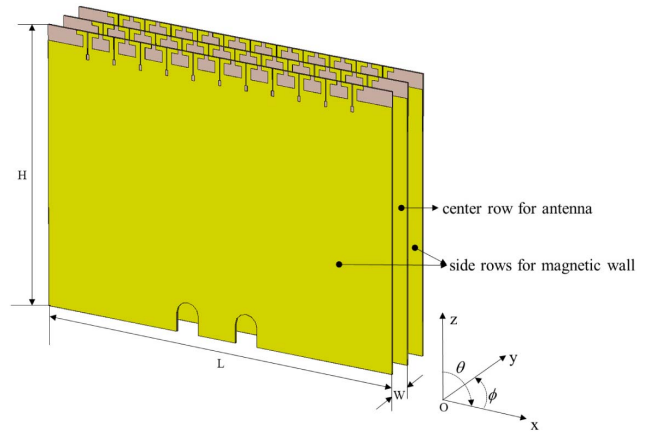


Fig. 12. Geometry of 11×3 basic T-printed dipole array for a finite AEP.

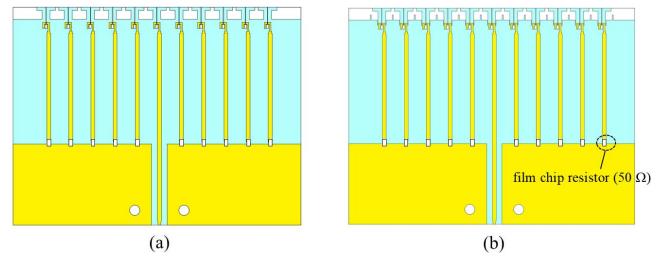


Fig. 13. Structure of an AEP of the 11×3 array. (a) Basic printed dipole. (b) Proposed.

that the resonant frequencies are shifted to a value lower than when only the stub structures are present.

V. FINITE ARRAY AND MEASUREMENTS

A. Physical Explanation for Finite Array

In Section III, the scan blindness mechanism for infinite arrays of a T-printed dipole has been discussed. Using stubs and slits, the scan blindness phenomenon is improved for the E-plane, but there is almost no pattern change for the H-plane. Therefore, for the purpose of measuring only the E-plane, the geometry of an 11×3 basic T-printed dipole array for a finite AEP is proposed in Fig. 12. The design parameters are $L = 42$ mm, $W = 30$ mm, and $D = 4.28$ mm. First, two types of 11×3 finite T-printed dipole arrays are illustrated in Fig. 12. The AEP structures based on the basic printed dipole model and the proposed elements are presented in Fig. 13(a) and (b), respectively. For AEP implementation, a center element of the middle row substrate is excited, and all other elements are matched and terminated with 50Ω thin-film chip resistors (0402 size, Vishay). Similarly, all elements of the first and third substrates are matched and terminated with 50Ω chip resistors, so that the two substrates worked as a magnetic wall. The other two types of antennas consist of 10×3 elements, but these operate as an 8×1 array. The substrate located in the middle row consists of eight excited elements and two matched terminated elements. In the case of a finite array, the AEP of the element near the edge differs from that of the center element [32]. Therefore, the edge elements of the substrate are used as dummy elements to preserve the uniformity of

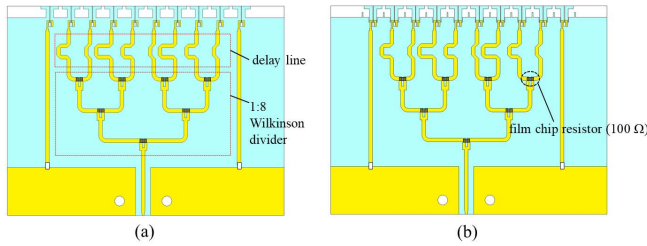
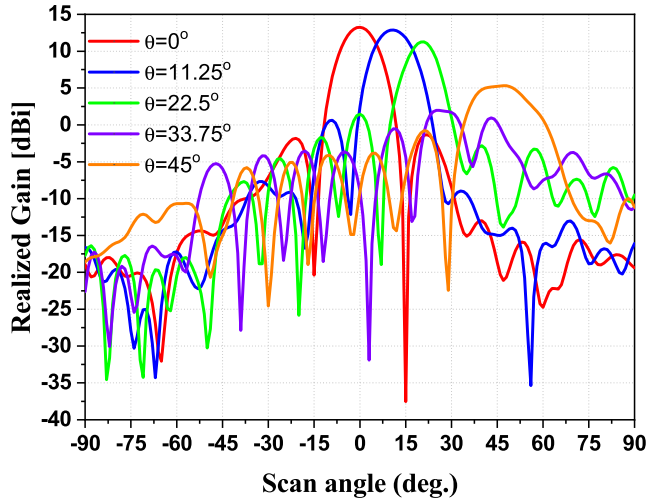
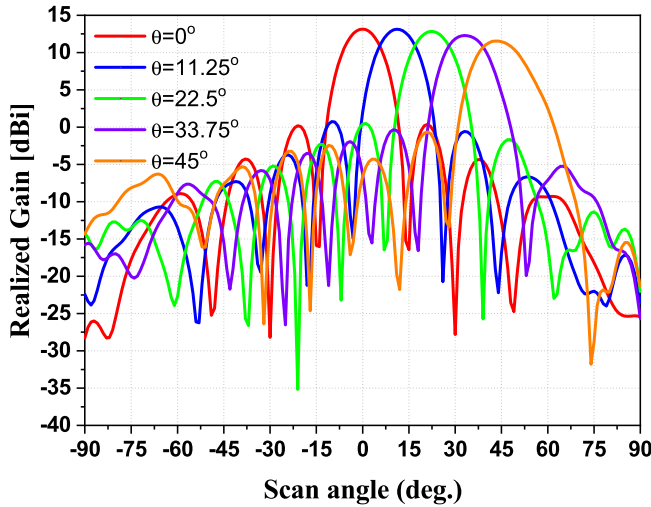


Fig. 14. Structure of fully excited 8×1 arrays in the E-plane with 41° scan angle. (a) Basic printed dipole. (b) Proposed.



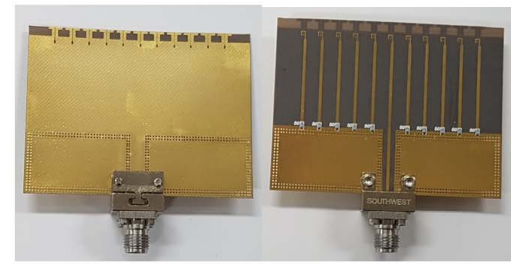
(a)



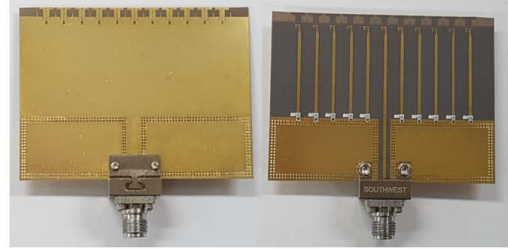
(b)

Fig. 15. Simulated scanning performance in the E-plane for the 11×3 arrays with an excited eight-element linear array. (a) Basic printed dipole. (b) Proposed.

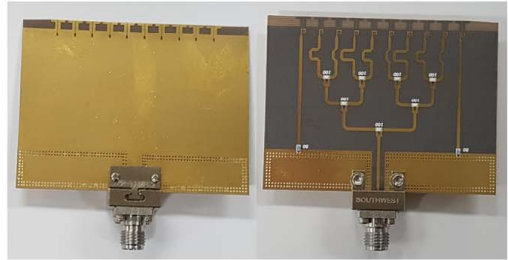
the AEP of the feeding elements, as shown in Fig. 14 [33]. Elements of the first and third rows of the array are terminated with 50Ω , similar to the AEP structures. The design model in Fig. 14(a) is realized as a basic printed dipole array and the second one in Fig. 14(b) depicts a printed dipole array with slits and stubs. A 1:8 Wilkinson divider is designed for Floquet excitation so that each element is isolated and excited



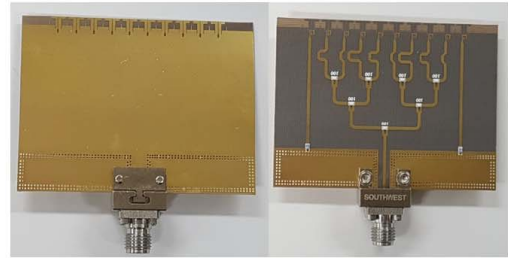
(a)



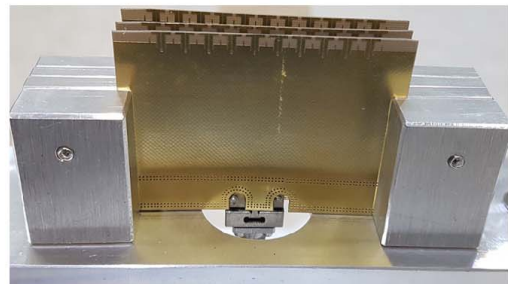
(b)



(c)



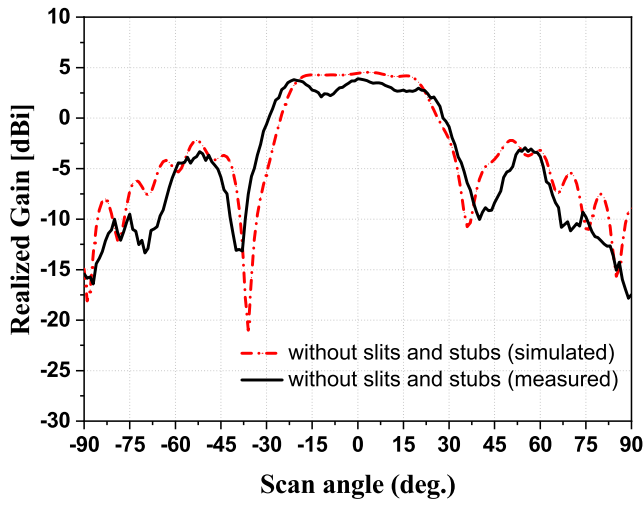
(d)



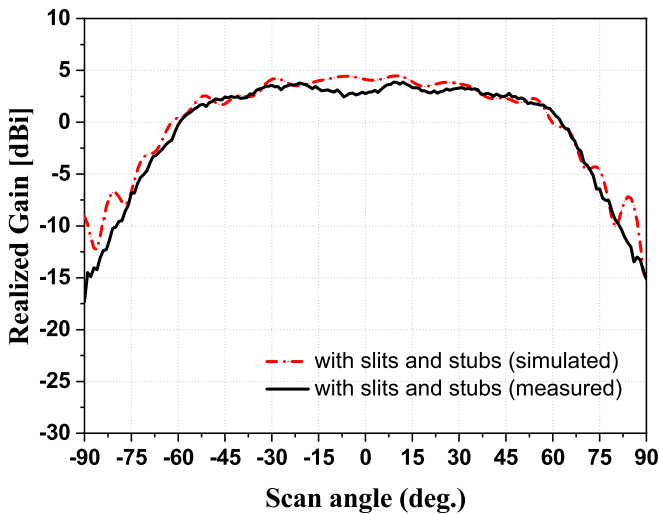
(e)

Fig. 16. Four types of center row substrate arrays fabricated. (a) AEP of the 11×3 arrays for the basic T-printed dipole. (b) AEP of the 11×3 arrays for the proposed T-printed dipole. (c) Fully excited 8×1 arrays for the basic T-printed dipole. (d) Fully excited 8×1 arrays for the proposed T-printed dipole. (e) Array of printed dipoles with slits and stubs mounted on the antenna bracket.

uniformly. The microstrip delay line in the feeding is a phase shifter. The phase difference of each device is 120° at 35 GHz, making the scan angle of the designed array 41° , which is



(a)



(b)

Fig. 17. E-plane co-polarization AEP of the 11×3 arrays. (a) Basic printed dipole. (b) Proposed.

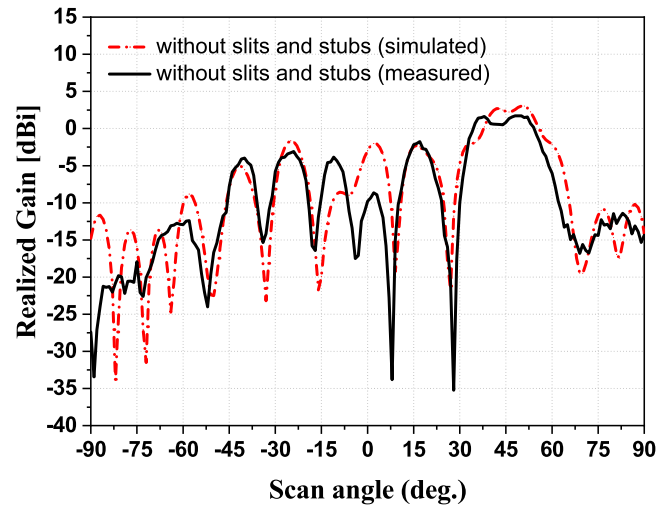
close to the scan blind angle of 36° . Chip resistors are used for matched termination, similar to the finite-AEP structure mentioned above.

B. Scanning Performance

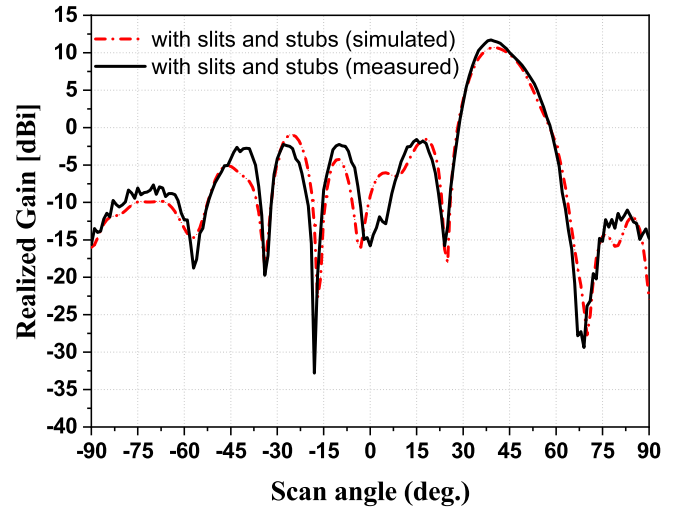
Fig. 15 shows the scanning performance of the 11×3 arrays with an excited eight-element linear array for the basic printed dipole and proposed printed dipole. The array is fed to the same amplitude and scanned at 11.25° intervals by controlling the phases at eight ports. In Fig. 15(a), when the scan angle is 33.75° near the scan blind angle, the co-polarization realized gain pattern is deteriorated by the scan blindness effect. On the contrary, the pattern is improved as shown in Fig. 15(b), using the slits and the stubs.

C. Simulations and Measurements

As explained in Section V-A, four types of prototypes were fabricated and measured. Fig. 16(a)–(d) shows the front and back views of the center row substrates with end launch



(a)



(b)

Fig. 18. Fully excited 8×1 arrays in the E-plane co-polarization at 41° scan angle. (a) Basic printed dipole. (b) Proposed.

connectors (type 2.92 mm). Fig. 16(e) depicts a photograph of the 11×3 T-printed dipole array with slits and stubs for finite AEP mounted on an antenna bracket made of aluminum. To validate the simulation results, experiments were performed in a far-field anechoic chamber. Fig. 17(a) and (b) presents the finite AEP simulated and measured in the E-plane at a fixed frequency for a basic T-printed dipole array and the proposed array, respectively. Scan blindness around $\pm 36^\circ$ is observed in both the measured and simulated results in Fig. 17(a). Fig. 17(b) illustrates that the scan blindness is eliminated in the AEP. The scan range of the AEP is $\pm 57^\circ$. At the broad side, the realized gain is 4.1 and 2.8 dBi for the simulated and measured values, respectively. Although a slight gain variation occurred in the measurement results owing to the scattering of the antenna bracket, the measured patterns are in good agreement with the simulated patterns. The measured and simulated realized gains were obtained as illustrated in Fig. 18, which shows the fully excited array for scanning toward 41° in the E-plane. Fig. 18(a) shows that the main beam is distorted because of the scan blindness. By adding a parasitic

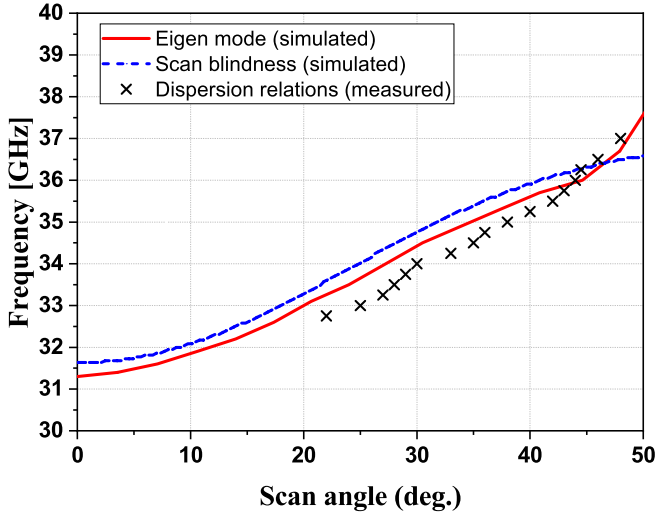


Fig. 19. Comparison of scan blindness occurrences when the printed dipole array antenna is steering from broadside to 50° in the E-plane. Eigen mode (simulated) versus dispersion relations (calculated) versus scan blindness (measured).

element, as shown in Fig. 18(b), the gain measured is improved by 9 dB compared to the original model. At the intended angle (41°), the realized gain is 10.6 and 11.7 dBi for the simulated and measured values, respectively. Fig. 19 shows the measurements of the scan blindness traces for E-plane scanning obtained by sweeping the frequencies from 32.5 to 37 GHz with 0.25 GHz intervals. The measured data are matched with the eigen modes simulated for a basic T-printed dipole. From the results in Fig. 19, it can be inferred that the quasi-TEM wave guided along a row of T-printed dipole elements is the main cause of the scan blindness.

VI. CONCLUSION

In this article, the scan blindness in the T-printed dipole was analyzed and an elimination technique proposed. The main cause of the scan blindness was found to be a quasi-TEM guided wave mode traveling along the printed dipole substrate in the E-plane through an infinite rectangular array. The existence of a guided wave was analyzed by confirming that the eigen mode and scan blindness curves are identical. Moreover, this mode could be predicted using a proposed simple equivalent circuit and a dispersion relation formula. Through this equation, it was verified that this guiding wave can be described as a quasi-TEM mode. It was also found that adding slits and stubs in the unit cell plays an important role in lowering the resonant frequencies in the printed dipole structure. Therefore, it could be considered an efficient method for eliminating the scan blindness at the desired frequencies. The analysis was verified by simulations and experiments conducted on four types of models, AEP, and array prototype with and without parasitic structures. The proposed concept provides improvements in the gain and scan range. The analysis of the scan blindness and its elimination method can be applied to various types of half-wave dipole antennas with balun in a rectangular array. The analysis of the scan

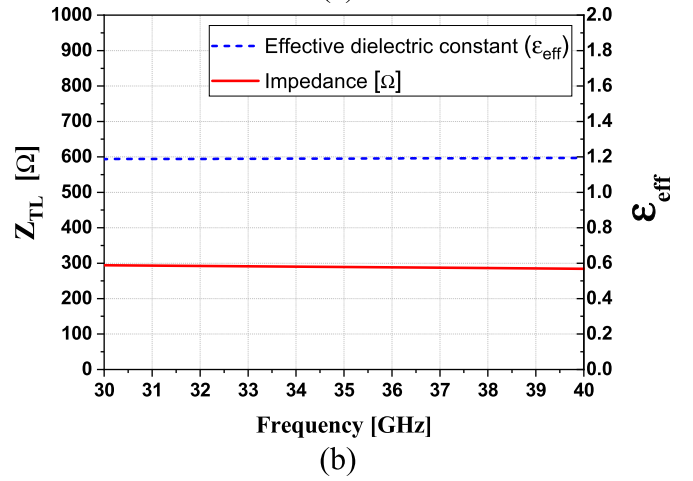
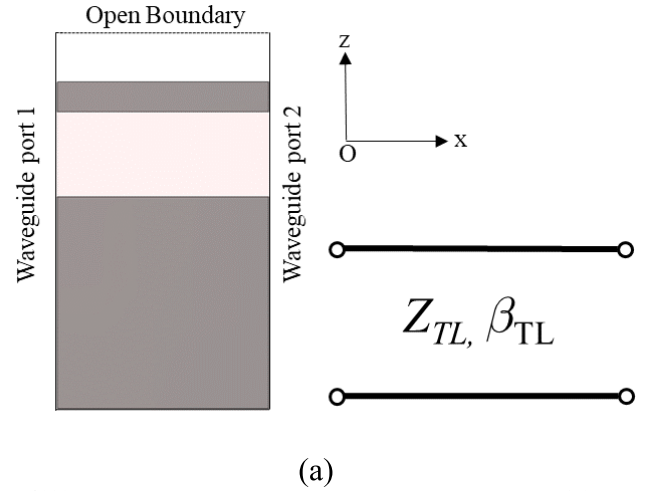


Fig. 20. Extraction of TL parameters. (a) Simulation setup for TL parameters. (b) Characteristic impedance Z_{TL} and phase constant β_{TL} .

blindness will be extended to other lattice configurations of dipole antennas in future work.

APPENDIX

DERIVATION OF DISPERSION RELATIONS

In this appendix, the derivation of dispersion relations and the method of the components extractions are introduced from the equivalent circuit of the T-printed dipole unit cell shown in Fig. 6. Each element in Fig. 6(b) is expressed in terms of the ABCD parameters as T

$$T_{CapL} = \begin{bmatrix} 1 & \frac{1}{j2\omega C_{gs}} \\ 0 & 1 \end{bmatrix} \begin{bmatrix} 1 & 0 \\ \frac{1}{j2\omega C_{gp}} & 1 \end{bmatrix} \quad (3)$$

$$\beta_{unit} = k_0 \sin \theta_{scan} \quad (4)$$

$$T_{CapR} = \begin{bmatrix} 1 & 0 \\ \frac{1}{j2\omega C_{gp}} & 1 \end{bmatrix} \begin{bmatrix} 1 & \frac{1}{j2\omega C_{gs}} \\ 0 & 1 \end{bmatrix} \quad (5)$$

$$T_{TL} = \begin{bmatrix} \cos \psi & jZ_{TL} \sin \psi \\ jY_{TL} \sin \psi & \cos \psi \end{bmatrix} \quad (6)$$

In this case, the phase of the TL (ψ) is given by

$$\psi = \beta_{TL} d_{TL} = \frac{2\pi \sqrt{\epsilon_{eff}}}{\lambda_0} d_{TL} \quad (7)$$

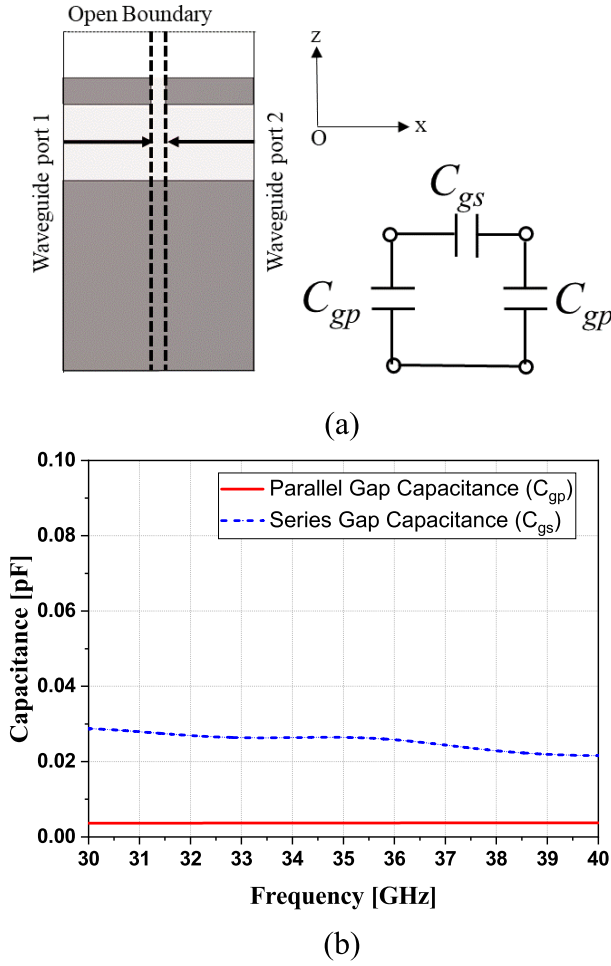


Fig. 21. Extraction of gap capacitance parameters. (a) Simulation setup for gap capacitance parameters. (b) Gap capacitance for series (C_{gs}) and gap capacitance for parallel (C_{gp}).

where the length of the dipole arm (d_{TL}) is 1.3925 mm

$$\begin{aligned}
 T_{TL} &= \begin{bmatrix} \frac{1}{j\omega C_{tp}} & 0 \\ 1 & 1 \end{bmatrix} \begin{bmatrix} A_{TF'} & B_{TF'} \\ C_{TF'} & D_{TF'} \end{bmatrix} \begin{bmatrix} \frac{1}{j\omega C_{tp}} & 0 \\ 1 & 1 \end{bmatrix} \quad (8) \\
 T_{TL} &= \begin{bmatrix} A_{TF'} & B_{TF'} \\ C_{TF'} & D_{TF'} \end{bmatrix} \\
 &= \begin{bmatrix} \frac{-y_{22,TF'}}{y_{21,TF'}} & \frac{-1}{y_{21,TF'}} \\ \frac{y_{12,TF'}y_{21,TF'} - y_{11,TF'}y_{22,TF'}}{y_{21,TF'}} & \frac{-y_{11,TF'}}{y_{21,TF'}} \end{bmatrix} \\
 Y_{11,TL'} &= j\omega C_{ts} + \frac{L}{j\omega(L - L_m)(1 + 2L_m)} \\
 Y_{21,TL'} &= -j\omega C_{ts} + \frac{L_m}{j\omega(L - L_m)(1 + 2L_m)} \\
 Y_{12,TL'} &= -j\omega C_{ts} + \frac{L_m}{j\omega(L - L_m)(1 + 2L_m)} \\
 Y_{22,TL'} &= j\omega C_{ts} + \frac{L}{j\omega(L - L_m)(1 + 2L_m)}. \quad (9)
 \end{aligned}$$

The unit cell matrix T_{unit} is expressed as follows:

$$T_{unit} = T_{CapL} T_{TL} T_{TF} T_{TL} T_{CapR}. \quad (10)$$

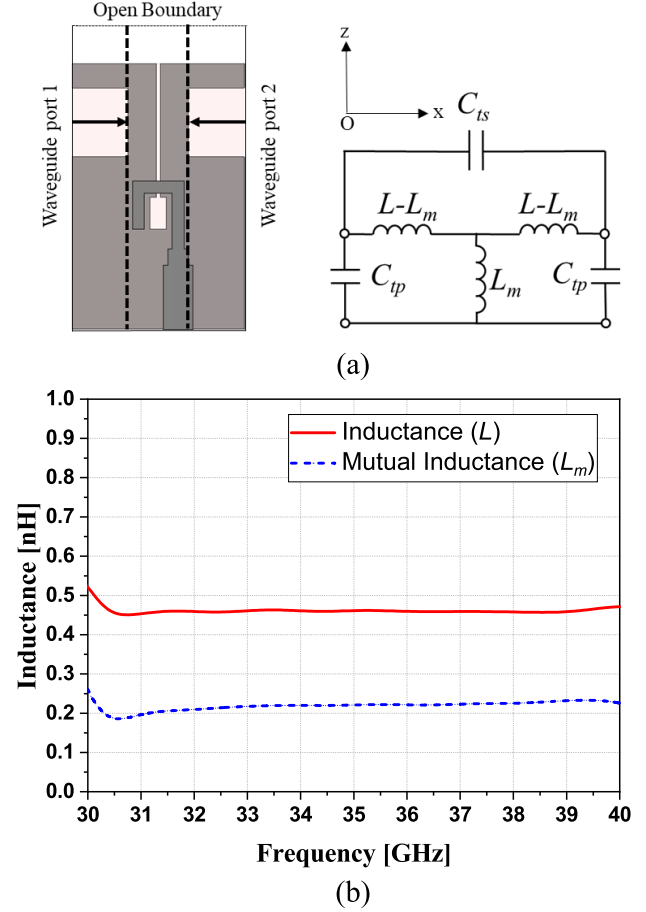


Fig. 22. Extraction of transformer parameters. (a) Simulation setup for transformer parameters. (b) Self-inductance (L) and mutual inductance (L_m).

According to the dispersion relation theory, (10) can be derived as

$$\cos \beta_{unit} a = 2B_{unit} C_{unit} + 1. \quad (11)$$

Using (2) and (12), the dispersion relation is expressed as

$$\cos k_0 a \sin \theta_{scan} = 2B_{unit} C_{unit} + 1. \quad (12)$$

In principle, any EM simulator can simulate the two-port network parameters of a unit cell. Each values of components in unit cell are determined by field distribution, geometry, and the boundary conditions. Since the boundary in the y-direction of the unit cell does not have phase differences, it acts as an H-wall.

A. Transmission Line

The arm of the T-printed dipole operates as a TL as shown in Fig. 20(a). The values of impedance (Z_{TL}) and the effective dielectric constant (ϵ_{eff}) obtained by exciting the waveguide port at both ends are shown in Fig. 20(b).

B. Capacitance

The lumped capacitance can be extracted from the Y matrix for a Pi-type network. The waveguide ports at both ends are

de-embedded by the length of the TL as shown in Fig. 21(a). Using (13)–(15), we obtain the gap capacitances as shown in Fig. 21(b)

$$Y_{Cap} = \begin{bmatrix} Y_{11,Cap} & Y_{12,Cap} \\ Y_{21,Cap} & Y_{22,Cap} \end{bmatrix} \quad (13)$$

$$C_{gs} = -\frac{\text{Im}(Y_{21,Cap})}{\omega_0} \quad (14)$$

$$C_{gp} = -\frac{\text{Im}(Y_{11,Cap} + Y_{21,Cap})}{\omega_0}. \quad (15)$$

C. Transformer

Like capacitance, each component of the transformer can be calculated from the Z matrix extracted from the simulation. The self-inductance (L) and the mutual inductance (L_m) can be derived from (9), but the appropriate parasitic shunt capacitance (C_{tp}) and parasitic series capacitance (C_{ts}) values need to be determined. The parameter study determines the appropriate C_{tp} so that the L has an independent value for the frequency. In the same way, C_{ts} associated with the L_m can be determined. Fig. 22(a) shows the transformer geometry de-embedded by the length of the TL, and the mutual inductance and the self-inductance can be calculated as Fig. 22(b). The values of the components are calculated as follows: $Z_{TL} = 288 \Omega$, $\epsilon_{\text{eff}} = 1.19$, $C_{gs} = 0.026$ pF, $C_{gp} = 0.004$ pF, $C_{tp} = 0.01$ pF, $C_{ts} = 0.02$ pF, $L = 0.46$ nH, and $L_m = 0.24$ nH.

REFERENCES

- [1] A. K. Bhattacharyya, *Phased Array Antennas: Floquet Analysis, Synthesis, BFNs and Active Array Systems*. Hoboken, NJ, USA: Wiley, 2006.
- [2] D. M. Pozar and D. H. Schaubert, "Scan blindness in infinite phased arrays of printed dipoles," *IEEE Trans. Antennas Propag.*, vol. AP-32, no. 6, pp. 602–610, Jun. 1984.
- [3] D. M. Pozar and D. H. Schaubert, "Analysis of an infinite array of rectangular microstrip patches with idealized probe feeds," *IEEE Trans. Antennas Propag.*, vol. AP-32, no. 10, pp. 1101–1107, Oct. 1984.
- [4] D. M. Pozar, "Analysis of finite phased arrays of printed dipoles," *IEEE Trans. Antennas Propag.*, vol. AP-33, no. 10, pp. 1045–1053, Oct. 1985.
- [5] D. M. Pozar, "Finite phased arrays of rectangular microstrip patches," *IEEE Trans. Antennas Propag.*, vol. AP-34, no. 5, pp. 658–665, May 1986.
- [6] J.-P. R. Bayard, "Analysis of infinite arrays of microstrip-fed dipoles printed on protruding dielectric substrates and covered with a dielectric radome," *IEEE Trans. Antennas Propag.*, vol. 42, no. 1, pp. 82–89, Jan. 1994.
- [7] J.-P. R. Bayard and M. E. Cooley, "Scan performance of infinite arrays of microstrip-fed dipoles with bent arms printed on protruding substrates," *IEEE Trans. Antennas Propag.*, vol. 43, no. 8, pp. 884–888, Aug. 1995.
- [8] D. H. Schaubert, "A class of E-plane scan blindnesses in single-polarized arrays of tapered-slot antennas with a ground plane," *IEEE Trans. Antennas Propag.*, vol. 44, no. 7, pp. 954–959, Jul. 1996.
- [9] A. Ellgardt, "A scan blindness model for single-polarized tapered-slot arrays in triangular grids," *IEEE Trans. Antennas Propag.*, vol. 56, no. 9, pp. 2937–2942, Sep. 2008.
- [10] Y. Fu and N. Yuan, "Elimination of scan blindness of microstrip phased array using electromagnetic bandgap structures," *IEEE Antennas Wireless Propag. Lett.*, vol. 3, pp. 63–65, 2004.
- [11] L. Zhang, J. A. Castaneda, and N. G. Alexopoulos, "Scan blindness free phased array design using PBG materials," *IEEE Trans. Antennas Propag.*, vol. 52, no. 8, pp. 2000–2007, Aug. 2004.
- [12] G. Donzelli, F. Capolino, S. Boscolo, and M. Midrio, "Elimination of scan blindness in phased array antennas using a grounded-dielectric EBG material," *IEEE Antennas Wireless Propag. Lett.*, vol. 6, pp. 106–109, 2007.
- [13] S. S. Holland, "Modeling of photonic bandgap effects on scan blindnesses in printed dipole array," in *Proc. Int. Symp. Antennas Propag. (APSURSI)*, Jul. 2017, pp. 1589–1590.
- [14] E. Adas, F. De Flaviis, and N. G. Alexopoulos, "Realization of scan blindness free finite microstrip phased arrays based on mode-free radiating electromagnetic bandgap materials," *IEEE Trans. Antennas Propag.*, vol. 66, no. 7, pp. 3375–3382, Jul. 2018.
- [15] Z. Xu, C. Zhang, T. Kaufmann, X. Yan, Y. Yuan, and C. Fumeaux, "Analysis of scan blindness in a linearly polarized tapered-slot phased array in triangular lattice—Performance improvement with parasitic notches," *IEEE Trans. Antennas Propag.*, vol. 62, no. 8, pp. 4057–4066, Aug. 2014.
- [16] J. T. Logan, R. W. Kindt, and M. N. Vouvakis, "A 1.2–12 GHz sliced notch antenna array," *IEEE Trans. Antennas Propag.*, vol. 66, no. 4, pp. 1818–1826, Apr. 2018.
- [17] C. Sabatier, "T-dipole arrays for mobile applications," *IEEE Antennas Propag. Mag.*, vol. 45, no. 6, pp. 9–26, Dec. 2003.
- [18] Y.-H. Suh and K. Chang, "A new millimeter-wave printed dipole phased array antenna using microstrip-fed coplanar stripline tee junctions," *IEEE Trans. Antennas Propag.*, vol. 52, no. 8, pp. 2019–2026, Aug. 2004.
- [19] Q.-Q. He, B.-Z. Wang, and J. He, "Wideband and dual-band design of a printed dipole antenna," *IEEE Antennas Wireless Propag. Lett.*, vol. 7, pp. 1–4, 2008.
- [20] H.-W. Yuan, S.-X. Gong, P.-F. Zhang, and X. Wang, "Wide scanning phased array antenna using printed dipole antennas with parasitic element," *Prog. Electromagn. Res. Lett.*, vol. 2, pp. 187–193, 2008.
- [21] R. L. Li, B. Pan, T. Wu, K. Lim, J. Laskar, and M. M. Tentzeris, "Equivalent-circuit analysis and design of a broadband printed dipole with adjusted integrated balun and a printed array for base station applications," *IEEE Trans. Antennas Propag.*, vol. 57, no. 7, pp. 2180–2184, Jul. 2009.
- [22] R. A. Alhalabi and G. M. Rebeiz, "High-efficiency angled-dipole antennas for millimeter-wave phased array applications," *IEEE Trans. Antennas Propag.*, vol. 56, no. 10, pp. 3136–3142, Oct. 2008.
- [23] S. X. Ta, H. Choo, and I. Park, "Broadband printed-dipole antenna and its arrays for 5G applications," *IEEE Antennas Wireless Propag. Lett.*, vol. 16, pp. 2183–2186, 2017.
- [24] S. X. Ta and I. Park, "Broadband printed-dipole antennas for millimeter-wave applications," in *Proc. IEEE Radio Wireless Symp.*, Phoenix, AZ, USA, Jan. 2017, pp. 65–67.
- [25] D. Sievenpiper, L. Zhang, R. F. J. Broas, N. G. Alexopoulos, and E. Yablonovitch, "High-impedance electromagnetic surfaces with a forbidden frequency band," *IEEE Trans. Microw. Theory Techn.*, vol. 47, no. 11, pp. 2059–2074, Nov. 1999.
- [26] F. Elek and G. V. Eleftheriades, "Dispersion analysis of the shielded Sievenpiper structure using multiconductor transmission-line theory," *IEEE Microw. Wireless Compon. Lett.*, vol. 14, no. 9, pp. 434–436, Sep. 2004.
- [27] D. M. Pozar, "The active element pattern," *IEEE Trans. Antennas Propag.*, vol. 42, no. 8, pp. 1176–1178, Sep. 1994.
- [28] D. M. Pozar, *Microwave Engineering*, 4th ed. New York, NY, USA: Wiley, 2011, pp. 288–293.
- [29] G. V. Eleftheriades, A. K. Iyer, and P. C. Kremer, "Planar negative refractive index media using periodically L-C loaded transmission lines," *IEEE Trans. Microw. Theory Techn.*, vol. 50, no. 12, pp. 2702–2712, Dec. 2002.
- [30] S. Raza, "Characterization of the reflection and dispersion properties of mushroom-related structures and their application to antennas," M.S. thesis, Dept. Elect. Comput. Eng., Univ. Toronto, Toronto, Canada, 2012.
- [31] S. Lim, W. Choi, and Y. Yoon, "Miniaturized radio frequency choke using modified stubs for high isolation in MIMO systems," *J. Electromagn. Eng. Sci.*, vol. 15, no. 4, pp. 219–223, Oct. 2015.
- [32] A. K. Bhattacharyya, "Active element pattern symmetry for asymmetrical element arrays," *IEEE Antennas Wireless Propag. Lett.*, vol. 6, pp. 275–278, 2007.
- [33] E. Holzman, "On the use of dummy elements to match edge elements in transmit arrays," in *Proc. IEEE Int. Symp. Phased Array Syst. Technol.*, Oct. 2013, pp. 549–552.
- [34] CST Corporation. (2018). *CST Microwave Studio (MWS)*. [Online]. Available: <http://www.cst.com>



Hanni Koo received the B.S. and M.S. degrees in radio science and engineering from Chungnam National University, Daejeon, South Korea, in 2006 and 2008, respectively. He is currently pursuing the Ph.D. degree with Seoul National University, Seoul, South Korea.

From 2008 to 2015, he was a Researcher with VICTEK Research Laboratory, Icheon-si, South Korea. His current research interest includes microwave and millimeter-wave antenna design and analysis.



Sangwook Nam (S'87–M'88–SM'11) received the B.S. degree in electrical engineering from Seoul National University, Seoul, South Korea, in 1981, the M.S. degree in electrical engineering from the Korea Advanced Institute of Science and Technology, Seoul, in 1983, and the Ph.D. degree in electrical engineering from The University of Texas at Austin, Austin, TX, USA, in 1989.

From 1983 to 1986, he was a Researcher with the Gold Star Central Research Laboratory, Seoul. Since 1990, he has been a Professor with the School of Electrical Engineering and Computer Science, Seoul National University. His current research interests include analysis/design of electromagnetic structures, antennas, and microwave active/passive circuits.